The Astrophysical Journal, 868:18 (8pp), 2018 November 20 https://doi.org/10.3847/1538-4357/aae5f6


# Three-dimensional Oscillations of 21 Halo Coronal Mass Ejections Using Multi-spacecraft Data

Harim Lee[1], Y.-J. Moon[1,2], V. M. Nakariakov[1,3], Hyeonock Na[1], Il-Hyun Cho[2], and Eunsu Park[1]
[1] School of Space Research, Kyung Hee University, Yongin 17104, Republic of Korea; moonyj@khu.ac.kr
[2] Department of Astronomy and Space Science, Kyung Hee University, Yongin 17104, Republic of Korea
[3] Centre for Fusion, Space & Astrophysics, Physics Department, University of Warwick, Coventry CV4 7AL, UK
*Received 2018 July 30; revised 2018 September 30; accepted 2018 October 1; published 2018 November 14*

## Abstract

We investigate the 3D structure of kinematic oscillations of full halo coronal mass ejections (FHCMEs) using multi-spacecraft coronagraph data from two non-parallel lines of sight. For this, we consider 21 FHCMEs which are simultaneously observed by the *Solar and Heliospheric Observatory* and the *Solar TErrestrial RElations Observatory A* or *B*, from 2010 June to 2012 August when the spacecraft were roughly in quadrature. Using sequences of running difference images, we estimate the instantaneous projected speeds of the FHCMEs at 24 different azimuthal angles in the planes of the sky of those coronagraphs. We find that all these FHCMEs have experienced kinematic oscillations characterized by quasi-periodic variations of the instantaneous projected radial velocity with periods ranging from 24 to 48 min. The oscillations detected in the analyzed events are found to show distinct azimuthal wave modes. Thirteen events (about 62%) are found to oscillate with the azimuthal wave number $m = 1$. The oscillating directions of the nodes of the $m = 1$ mode for these FHCMEs are consistent with those of their position angles (or the direction of eruption), with a mean difference of about 23°. The oscillation amplitude is found to correlate well with the projected radial speed of the CME. An estimation of Lorentz accelerations shows that they are dominant over other forces, implying that the magnetic force is responsible for the kinematic oscillations of CMEs. However, we cannot rule out other possibilities: a global layer of enhanced current around the CMEs or the nonlinear nature of its driver, for example the effect of vortex shedding.

*Key words:* Sun: coronal mass ejections (CMEs) – Sun: oscillations

## 1. Introduction

Coronal mass ejections (CMEs) are the most spectacular eruptions from the Sun into the heliosphere. They are usually thought to be the main source of strong geomagnetic storms (e.g., Gosling et al. 1991; Gosling 1993). It is well known that the interplanetary propagation of CMEs is controlled by the ambient solar wind (e.g., Lindsay et al. 1999; Gopalswamy et al. 2000, 2001a, 2001b; Vršnak & Žic 2007). Several authors (e.g., Vršnak et al. 2004; Yashiro et al. 2004) have suggested that the interaction between CMEs and the solar wind is an important mechanism that determines CME kinematics.

Dynamical processes in the solar corona are often accompanied by the excitation of various kinds of oscillations of coronal plasma non-uniformities, with periods ranging from a fraction of a second to several hours. The majority of coronal oscillations have been identified as magnetohydrodynamic (MHD) modes of various plasma non-uniformities (see, e.g., De Moortel & Nakariakov 2012; Liu & Ofman 2014, for comprehensive reviews). The interest in MHD oscillations is related to many open questions, such as heating of the plasma, the presence of additional sinks for the energy released in flares, triggering the energy releases, and MHD seismology diagnostics of plasma parameters and physical processes operating in the plasma by means of MHD oscillations.

CMEs may be accompanied by MHD oscillations that appear naturally as the response of the elastic and compressive plasma to the energy deposition. The first observation of oscillations in CME kinematics was reported by Krall et al. (2001). Examining the evolution of the speed patterns of the leading-edge and trailing-edge features for a flux-rope-like CME, they found that the projected CME speeds varied with a period of about 4–6 hr. Shanmugaraju et al. (2010) examined the speed–distance profiles of 116 CMEs observed with at least 10 height–time data points, and found that about 15 CMEs had quasi-periodic oscillation patterns in the evolution of their speed. The oscillation periods were estimated to be within the range of the upper and lower limit of the Alfvén travel times along the magnetic ropes of the CMEs. Lee et al. (2015) presented the first detection of both radial and azimuthal oscillations in halo CMEs (HCMEs) observed by the Large Angle SpectrosCopic Observatory (LASCO) C3. They found that the instantaneous projected radial velocity varies quasi-periodically, with period ranging from 24 to 48 min, and that the oscillations of seven CMEs are associated with distinct $m = 1$ azimuthal wave modes, where $m$ is the azimuthal wave number. Michalek et al. (2016) performed a comprehensive statistical study on the kinematics of 187 limb CMEs observed with LASCO. They found that 22% of the CMEs observed between 1996 and 2004 revealed periodic variations of the projected radial acceleration and speed, with average amplitude 87 km $s^{-1}$, mean period 241 min, and wavelength 7.8 $R_{\odot}$.

Lee et al. (2015) suggested that the kinematic oscillations of CMEs could be associated with a "zigzag" trajectory of the plasmoid, caused by the periodic shedding of vortices from its alternate sides in the direction perpendicular to the path (Nakariakov et al. 2009). In this scenario, the oscillation period anti-correlates with the CME speed, which was found to be consistent with observations. Michalek et al. (2016) concluded that properties of CME oscillations are consistent with the thin magnetic rope oscillation model of Cargill et al. (1994). Recently, Takahashi et al. (2017) developed a theoretical model of quasi-periodic oscillations of CME ropes, based on time-dependent magnetic reconnection in eruptive flares. The

oscillation period was estimated as the ratio of the width of the reconnection outflow near the CME flux rope and the Alfvén speed in the inflow region near the stagnation point, multiplied by an empirically determined factor of about 20. This modeling demonstrated the possibility of an oscillatory behavior of the CME radial and expansion speeds with periods ranging from ten to several hundred minutes at a heliocentric distance of about $10\,R_{\odot}$. An important feature of this mechanism is the linear increase in the period with the distance from the Sun, which could be tested observationally.

Thus, many authors have shown a variety of oscillatory patterns in the CME kinematics using single-spacecraft observations, revealing that these are a common feature of CME propagation. Those findings are supported by the results of theoretical estimations and modeling. However, single-view observations do not provide information about the 3D structure of the oscillations, as coronagraphic observations of CMEs are subject to projection effects (see, e.g., Bronarska & Michalek 2018 for a recent discussion). In particular, it is not clear whether the apparent oscillatory variations of the projected speed of CMEs are radial or azimuthal, i.e., whether the oscillations are polarized along or across the CME propagation direction. There has been so far no attempt to make a simultaneous observation of 3D CME oscillations using imaging observations from different lines of sight (LoSs). In this paper, we present the first detection of both radial and azimuthal oscillations of full HCMEs using multi-spacecraft observations with non-parallel LoSs, and determination of their wave modes. The paper is organized as follows. In Section 2, we describe the data and analysis. Results are given in Section 3 and a brief summary and discussion are presented in Section 4.

## 2. Data

In this study, we consider full HCMEs (FHCMEs) observed by space-based coronagraphs such as the *Solar and Heliospheric Observatory* (*SOHO*)/LASCO C3 (Brueckner et al. 1995) and the *Solar TErrestrial RElations Observatory* (*STEREO*; Kaiser et al. 2008)/Sun–Earth Connection Coronal and Heliospheric Investigation (SECCHI) COR2 from 2011 June to 2012 August, when these space missions were approximately in quadrature. During this period of time, the angular separations of the *STEREO-A* and *-B* spacecraft from the Sun–Earth line were in the range 94°–123° and 93°–115°, respectively. The field of view of LASCO C3 is 3.7–30 $R_{\odot}$, and that of *STEREO* COR2 is 2–15 $R_{\odot}$.

We choose 21 well-observed FHCMEs whose front structures are clearly seen in both C3 and COR2, and whose evolution was traced by at least five consecutive measurements, made at heights from 3.2 to 26.8 $R_{\odot}$ with a time cadence of about 12–15 min. The dates, times, source locations, and other properties of the events are summarized in Table 1.

Figure 1 shows running difference images of the 2011 September 22 event, obtained with three satellites: *STEREO-B* COR2, LASCO C3, and *STEREO-A* COR2. For each running difference image, we estimate locations of the FHCME's front edge at every 15° of the azimuthal angle. The projected instantaneous speed $V_{\rm ins}$ of the FHCME was determined using two successive height–time measurements at every azimuthal angle.

Some uncertainties in determining the speed $V_{\rm ins}$ may exist because the determination of the HCME front edge locations are made by visual inspection. To estimate the uncertainty of the instantaneous speed estimation, we made ten independent trials of the measurements of the front edge locations, i.e., the technique used by Lee et al. (2015). Then the error is estimated as the standard deviation of those independent measurement, typically about 170 km $s^{-1}$.

To make the running difference images, we use level 0.5 data obtained by the LASCO/EIT Images Query Form (https://sharpp.nrl.navy.mil/cgi-bin/swdbi/lasco/images/form), and the SECCHI Flight images Query Form (https://secchi.nrl.navy.mil/cgi-bin/swdbi/secchi_flight/images/form).

## 3. Results and Discussion

Figure 2 gives an example of the instantaneous speed measurements, showing the speed as a function of time along different azimuths for the 2011 June 4 event, together with the best-fitting harmonic function. The speed is seen to quasi-periodically oscillate with distance from the Sun, rather than monotonically increase or decrease. The apparent oscillation was fitted by a harmonic function $V_{\rm ins} = \Delta V \sin(\omega(t - K)) + b$, where $\Delta V$ is the amplitude, $\omega$ is the cyclic frequency, $K$ is the phase, and $b$ is the mean value, which are determined by the least-squares method. Following this approach, we estimate the speed amplitudes $\Delta V$ at every azimuth angle, stepping by 15°, of all events. We restrict our attention to the data sets which have the absolute values of the cross-correlation coefficients with best-fitting harmonic functions larger than 0.6. For example, for the event shown in Figure 2, the CME speed evolution along a number of azimuthal rays positively correlates with the harmonic function, with a maximum cross-correlation coefficient $CC_{\rm max} = 0.99$ and a mean cross-correlation coefficient $CC_{\rm mean} = 0.91$. The speed variation along other azimuthal rays in this CME shows strong anti-correlation with this function, $CC_{\rm max} = -0.99$ and $CC_{\rm mean} = -0.90$. Following this procedure, we estimate instantaneous radial speeds at every 15° azimuthal direction, for 21 FHCMEs. We find that all the FHCMEs have oscillatory patterns in the instantaneous projected speeds. In addition, we estimate the maximum observed projected speeds $V_{\rm pro}$ of the FHCMEs, obtained from a linear fit of height–time data at every azimuthal angle. Parameters of the detected oscillations and the CME speeds are given in Table 1.

Figure 3 shows an example in which the oscillatory pattern of instantaneous projected speeds has a systematic azimuthal dependence. This dependence is different if observed from different LoSs with LASCO C3 and *STEREO-A* COR2 in the CME shown in the figure. To quantify the azimuthal dependence of the oscillatory patterns, we estimate it as a harmonic function $\exp(im\theta)$, where $\theta$ is the azimuthal angle and $m$ is an integer representing the azimuthal wave number, which is estimated by the following procedure: (1) according to the phase of the oscillations (see the left panels of Figure 3) we group the oscillations at all azimuthal angles into "positive," "negative," and "non-oscillatory" groups; (2) we position nodal lines between the azimuthal rays corresponding to the "positive" and "negative" groups; (3) the azimuthal mode number $m$ of the oscillation is obtained as the number of nodal lines. The instantaneous projected speed pattern along a given azimuthal angle is considered to belong to either the "positive" or "negative" group if it has a cross-correlation coefficient with the best-fitting harmonic functions either larger than 0.6 or smaller than −0.6, respectively. The oscillation position angle (OPA) is defined as the position angle of the direction that is

**Table 1**
Oscillation Parameters of 21 HCMEs

| Date (UT) | Time | Location | MPA (deg) | OPA (deg) | Duration (min) | | Distance ($R_\odot$) | | Projected Speed $V^{pro}$ (km s$^{-1}$) | | Speed Amplitude $\Delta V$ (km s$^{-1}$) | | Period (min) | | Mode ($m$) | | | *STEREO* |
|---|---|---|---|---|---|---|---|---|---|---|---|---|---|---|---|---|---|---|
| | | | | | L | S | L | S | L | S | L | S | L | S | L | S | Final | |
| 2011 Jun 4 | 06:48:06 | N16W144 | 284 | 195, 285 | 60 | 60 | 5.8–25.2 | 4.7–16.1 | 2128 | 2002 | 768 | 425 | 24 | 30 | 2 | 0 | 2 | *A* |
| 2011 Aug 4 | 04:12:05 | N19W36 | 298 | 300 | 120 | 60 | 5.1–24.7 | 3.8–15.1 | 2267 | 2185 | 717 | 539 | 24 | 30 | 1 | 1 | 1 | *A* |
| 2011 Sep 22 | 10:48:06 | N09E89 | 72 | 90 | 72 | 60 | 5.5–21.7 | 4.3–11.9 | 2510 | 2241 | 776 | 492 | 24 | 30 | 1 | 1 | 1 | *B* |
| 2011 Sep 24 | 12:48:07 | N10E56 | 78 | ⋯ | 72 | 75 | 4.9–27.0 | 3.9–15.7 | 2884 | 2163 | 967 | 695 | 24 | 30 | 0 | 1 | 1 | *A* |
| 2011 Oct 22 | 10:24:05 | N25W77 | 311 | ⋯ | 96 | 90 | 9.6–24.9 | 4.1–13.6 | 1669 | 1332 | 565 | 346 | 48 | 30 | 0 | 1 | 1 | *B* |
| 2011 Nov 26 | 07:12:06 | N17W49 | 327 | ⋯ | 120 | 60 | 6.4–25.5 | 3.6–15.8 | 1399 | 1639 | 506 | 563 | 48 | 30 | ⋯ | 0 | ⋯ | *A* |
| 2012 Jan 23 | 04:00:05 | N28W21 | 326 | 330 | 60 | 60 | 5.4–21.8 | 3.2–13.8 | 2576 | 2568 | 590 | 939 | 24 | 30 | 1 | 2 | 2 | *A* |
| 2012 Jan 26 | 04:36:05 | N41W84 | 327 | ⋯ | 60 | 60 | 4.9–25.7 | 3.3–11.6 | 2147 | 1744 | 756 | 482 | 24 | 30 | 0 | 1 | 1 | *A* |
| 2012 Jan 27 | 18:27:52 | N27W71 | 296 | 195, 285 | 48 | 60 | 4.9–26.7 | 5.2–14.9 | 2657 | 2318 | 702 | 552 | 24 | 30 | 2 | 1 | 2 | *B* |
| 2012 Mar 5 | 04:00:05 | N17E52 | 61 | ⋯ | 72 | 60 | 5.7–26.3 | 4.4–14.3 | 2451 | 1911 | 731 | 260 | 24 | 30 | 0 | 0 | 0 | *A* |
| 2012 Mar 10 | 18:00:05 | N17W24 | 5 | 45 | 108 | 75 | 5.3–19.4 | 3.8–12.1 | 1825 | 1265 | 483 | 325 | 24 | 30 | 1 | 1 | 1 | *A* |
| 2012 Mar 13 | 17:36:05 | N17W66 | 286 | 225 | 60 | 60 | 5.6–25.3 | 5.7–14.7 | 2398 | 1710 | 601 | 406 | 48 | 30 | 1 | 1 | 1 | *B* |
| 2012 Mar 18 | 00:24:05 | N18W116 | 300 | ⋯ | 120 | 60 | 4.8–25.3 | 5.6–14.7 | 1496 | 1869 | 409 | 453 | 48 | 30 | 0 | 1 | 1 | *A* |
| 2012 Mar 26 | 23:12:05 | N17E164 | 92 | 0, 90 | 48 | 60 | 4.2–15.4 | 6.8–16.4 | 1610 | 2022 | 430 | 422 | 24 | 30 | 2 | 1 | 2 | *B* |
| 2012 May 17 | 01:48:05 | N11W76 | 261 | ⋯ | 60 | 60 | 5.7–25.8 | 5.6–14.5 | 2170 | 1619 | 745 | 531 | 24 | 30 | ⋯ | 1 | ⋯ | *B* |
| 2012 Jun 14 | 14:12:07 | S17E06 | 144 | 120 | 120 | 60 | 5.3–17.6 | 3.8–14.7 | 1670 | 1777 | 567 | 360 | 24 | 30 | 1 | 1 | 1 | *A* |
| 2012 Jun 23 | 07:24:05 | S11E60 | 290 | ⋯ | 84 | 60 | 5.0–27.4 | 6.5–14.7 | 2238 | 1045 | 628 | 211 | 24 | 30 | ⋯ | 1 | ⋯ | *B* |
| 2012 Jul 06 | 23:24:06 | S13W59 | 233 | 255 | 48 | 60 | 5.0–26.8 | 5.3–16.0 | 2475 | 1949 | 828 | 454 | 48 | 30 | 1 | 0 | 1 | *B* |
| 2012 Jul 19 | 05:24:05 | S13W88 | 275 | 210 | 72 | 60 | 4.6–24.3 | 3.3–14.7 | 2199 | 2544 | 744 | 580 | 24 | 30 | 1 | 0 | 1 | *A* |
| 2012 Jul 23 | 02:36:05 | S17W132 | 286 | 270 | 72 | 60 | 4.4–24.7 | 4.6–15.7 | 2213 | 2598 | 644 | 458 | 24 | 30 | 1 | 0 | 1 | *A* |
| 2012 Aug 31 | 20:00:05 | S25E59 | 90 | 135 | 72 | 75 | 4.2–18.8 | 4.4–15.1 | 1717 | 1557 | 509 | 297 | 24 | 30 | 1 | 0 | 1 | *A* |

**Note.** Columns 1, 2: CME first appearance date and time in the LASCO C2 field of view. Columns 3, 4: CME source location and measurement position angle (MPA) reported in the CDAW LASCO CME catalog, respectively. Column 5: the CME oscillation position angle (OPA) in the LASCO C3 field of view. Columns 6–9: CME observing duration and distance range for LASCO (L) and *STEREO* (S). Columns 10–13: maximum projected CME speed ($V_{pro}$), and its oscillation amplitude ($\Delta V$) for L and S. Columns 14, 15: CME oscillation periods for L and S. Columns 16–19: azimuthal mode number of the CME oscillation for L, S, and combined. Column 20: *STEREO-A* or *-B*. If the field is blank (or has a dash), it means a rather complex wave pattern.

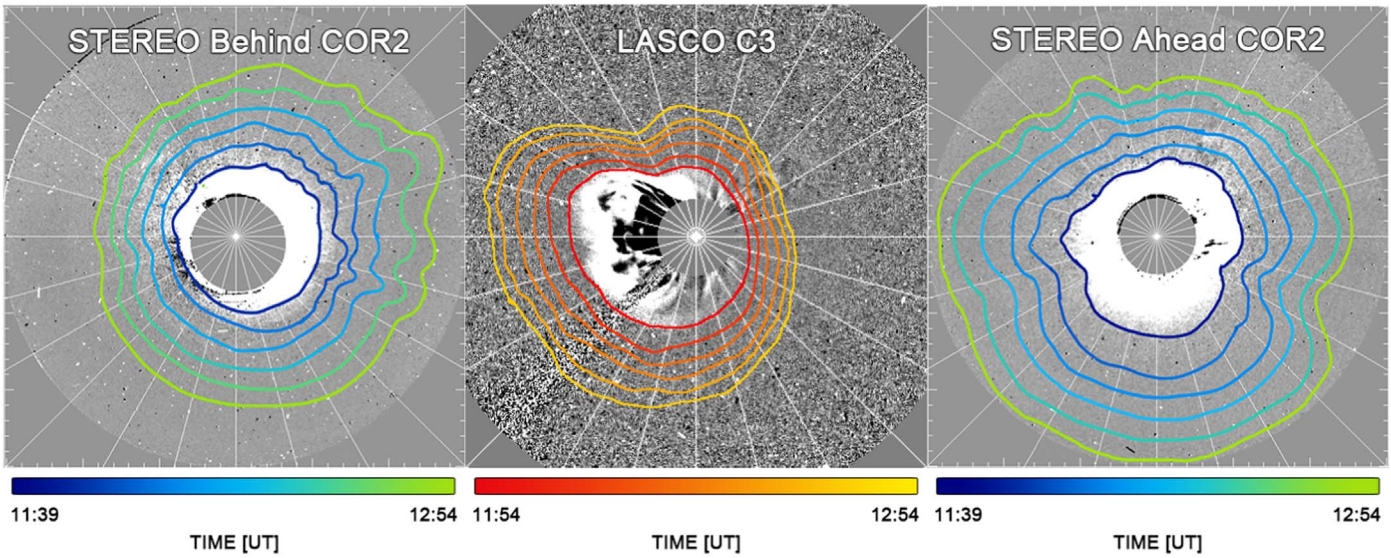


**Figure 1.** Running difference images of the 2011 September 22 FHCME at 11:39–12:54 UT. All measurements are made at every 15° (white lines). The color contour lines show the locations of the front edges of the FHCME from *STEREO B* COR2 (left), LASCO C3 (middle) and *STEREO A* COR2 (right).

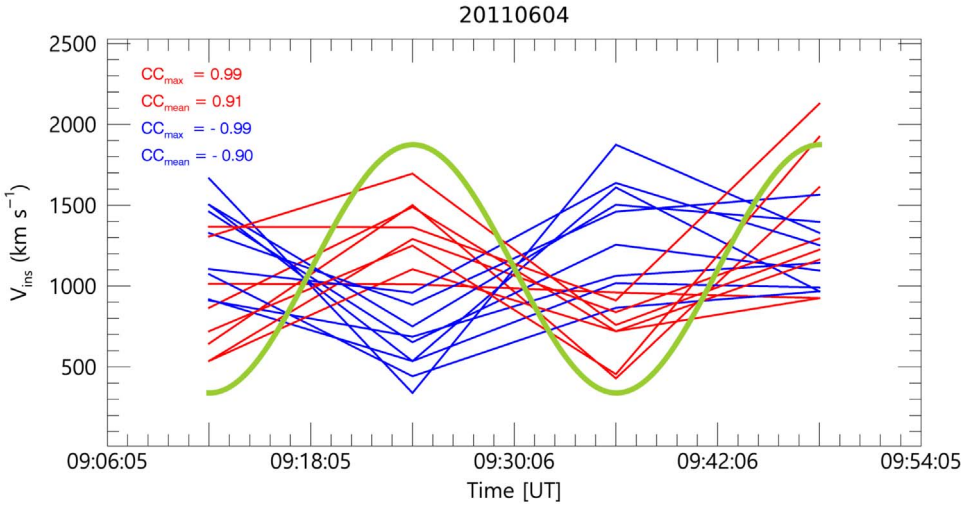


**Figure 2.** Profiles of the instantaneous projected speeds measured along different azimuthal angles in the 2011 June 4 FHCME. Only the speed profiles with the absolute values of the correlation coefficients with the harmonic function shown in green; values larger than 0.6 are shown. The red and blue lines show positive and negative correlations, respectively.

perpendicular to the nodal line for $m = 1$, and 45° from the nodal line for $m = 2$.

As seen in the left panel of Figure 3(a), the oscillatory patterns observed with LASCO C3 in all azimuthal angles have the same phase, and hence positively correlate with the same harmonic function. In the left panel of Figure 3(b), the oscillatory patterns observed with *STEREO-A* COR2 have, depending upon the azimuthal angle, two opposite phases. In the "positive" group of azimuths the oscillations correlate positively with a chosen harmonic function, while oscillations that belong to the "negative" group correlate with this function negatively. As seen in the right panel of Figure 3(b), the azimuthal distribution of the "positive" and "negative" groups observed with COR2 indicates the $m = 1$ mode. Thus, in this CME the oscillatory pattern observed with LASCO C3 corresponds to the $m = 0$ mode, while the oscillation observed from another LoS, with *STEREO-A* COR2, corresponds to the $m = 1$ mode. The oscillatory patterns are presented in more than 50% of the azimuthal angles. The observed maximum projected speeds are found to be about 2900 km s$^{-1}$ for LASCO C3 and about 2200 km s$^{-1}$ for *STEREO-A* COR2. The instantaneous speed oscillation amplitudes are estimated to be about 970 km s$^{-1}$ for LASCO C3 and about 700 km s$^{-1}$ for *STEREO-A* COR2. The oscillation period of the FHCME is about 24 min for LASCO C3 and 30 min for *STEREO-A* COR2.

Figure 4 gives an example of a CME with another azimuthal oscillatory pattern. As seen in the right panel, the oscillatory patterns are clearly presented for more than 50% of the azimuthal angles. The observed maximum projected speeds are found to be about 2700 km s$^{-1}$ for LASCO C3, and about 2300 km s$^{-1}$ for *STEREO-B* COR2. The instantaneous speed oscillation amplitudes are found to be about 700 km s$^{-1}$ for LASCO C3 and about 600 km s$^{-1}$ for *STEREO-B* COR2. The oscillation period of the FHCME is about 24 min for LASCO C3, and 30 min for *STEREO-B* COR2. As seen in the left panel, the oscillatory patterns have two opposite phases: positive correlations at some azimuthal angles and negative

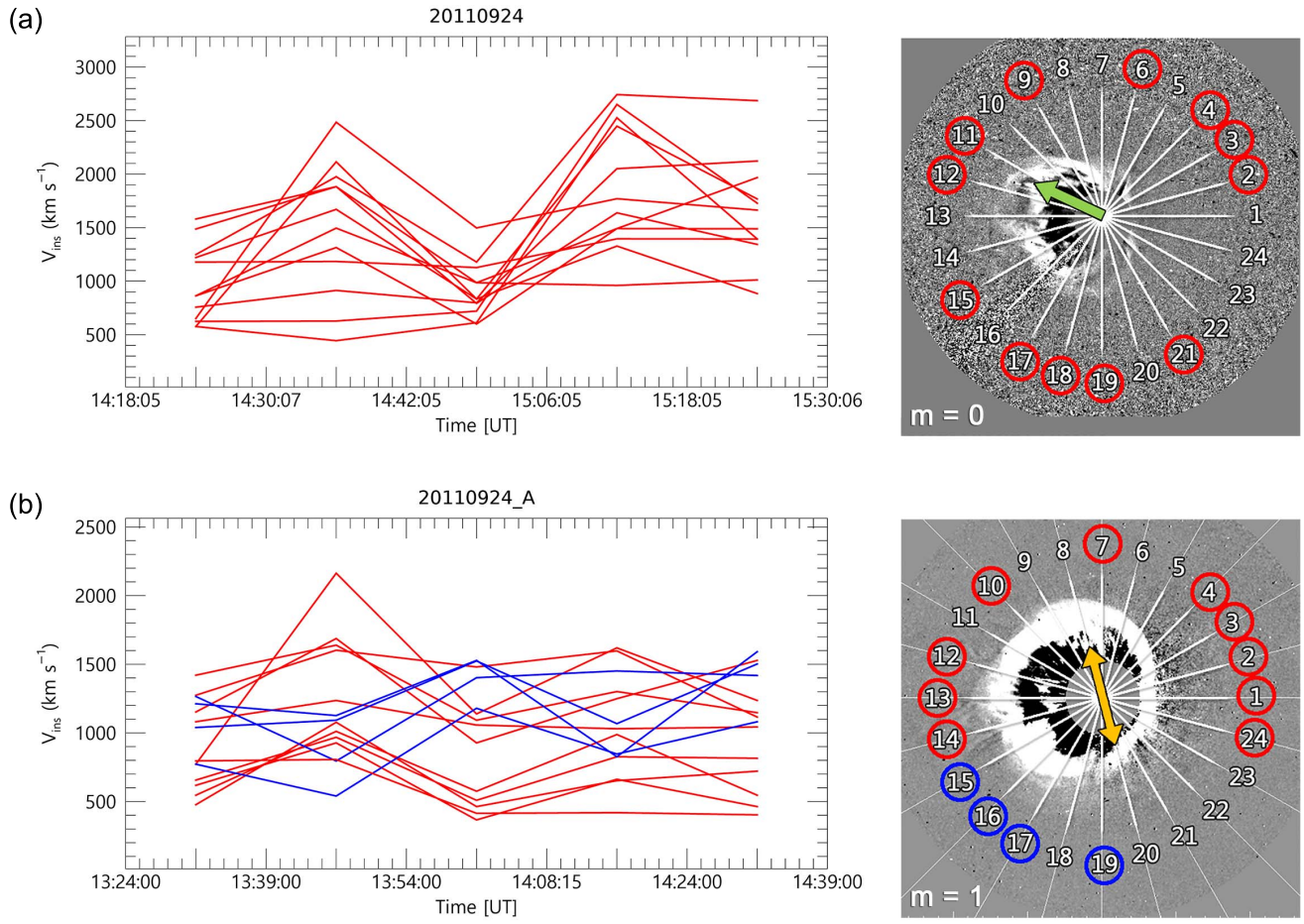


**Figure 3.** Oscillatory patterns in the 2011 September 24 FHCME (left), and their azimuthal dependences (right) observed with: (a) LASCO and (b) *STEREO-A*. In the left panels, the red and blue lines have the same meaning as in Figure 1. In the right panels, the red and blue circles indicate the azimuths in which the oscillations correlate either positively (red), or negatively (blue) with the best-fitting harmonic function. The yellow and green arrows show the OPAs and MPAs, respectively. In the left bottom panel the azimuthal mode numbers are indicated.

correlations at other angles with the same harmonic function. Thus, the oscillation observed in this event is likely of the $m = 2$ mode from the LASCO C3 LoS and the $m = 1$ mode from the COR2 LoS.

Figure 5 shows a sketch of the possible 3D structure of the kinematic oscillation of the FHCME shown in Figure 3. If the propagation direction of a CME and its oscillation direction are same, i.e., the oscillation is polarized in the radial (vertical) direction, and the CME is seen from the LoS parallel to this direction, the oscillatory patterns along each azimuth should have the same phase (i.e., $m = 0$; see the LASCO view in Figure 5). The same oscillatory pattern could look different if seen from another direction. In particular, the apparent oscillatory patterns on either sides of the CME may have opposite phases, i.e., positive phase at one side and negative phase at the other side ($m = 1$), if the LoS is perpendicular to the oscillation polarization direction; see the *STEREO* view in Figure 5. This shows that when the propagation direction is close to the oscillation direction, its wave mode is not properly identified in the coronagraph observation with the LoS parallel to the propagation direction. In particular, an $m = 1$ mode would be seen as an $m = 0$ mode. Therefore, in the identification of the oscillation mode we take a higher azimuthal mode out of two possible modes determined with different observational angles. Results obtained by this procedure for all 21 FHCMEs analyzed in this study are summarized in Table 1.

Figure 6(a) shows the relationship between the OPAs determined in this study and the MPAs (obtained from the LASCO catalog) that corresponds to the projected directions of solar eruptions. In this plot, we use 13 events (10 events for $m = 1$ and three events for $m = 2$), and neglect nine other events that either are of $m = 0$ or ambiguous. We find that the OPAs are quite consistent with the MPAs with a correlation coefficient of 0.92 and mean absolute difference of 23°. This finding indicates that the kinematic oscillations of these FHCMEs are mainly related to solar eruptions. Figure 6(b) shows the relationship between the oscillation amplitude and the maximum projected speed determined with LASCO C3. We find that there is a good correlation between these two quantities with a correlation coefficient of 0.80.

The net acceleration ($a_n$) of a CME consists of the combination of the Lorentz acceleration ($a_L$), gravitational acceleration ($g = 274/R^2$), and the aerodynamic drag acceleration ($a_d$) (Cargill et al. 1996; Cargill 2004; Vršnak et al. 2004, 2010):

$$a_n = a_L - g + a_d = a_L - g - \gamma(v - w)|v - w|, \quad (1)$$

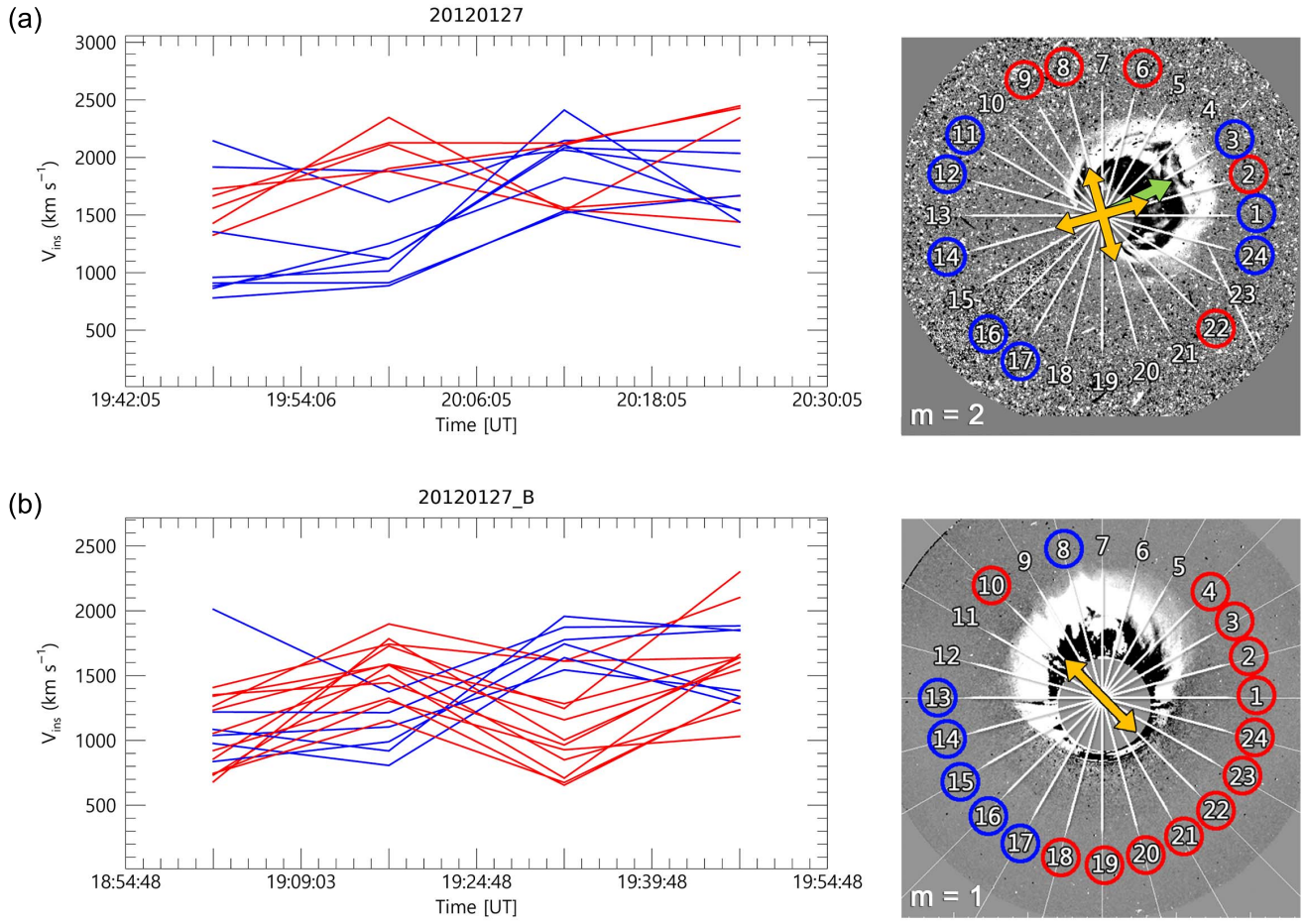


**Figure 4.** Oscillatory patterns of the 2012 January 27 FHCME (left) and its azimuthal dependence (right) observed with: (a) LASCO, and (b) *STEREO-B*. The notations are the same as in Figure 3.

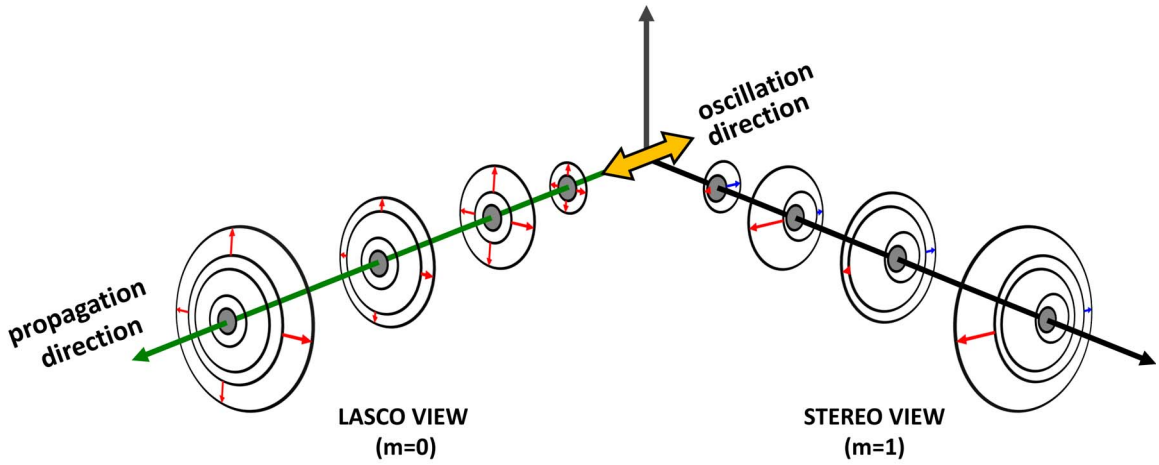


**Figure 5.** Simplified schematic diagram of the kinematic oscillation of the 2011 September 24 FHCME observed from different angles with two coronagraphs. The yellow arrow indicates the direction of the oscillation. The green arrow corresponds to the propagation direction of the FHCME. The red and blue arrows show the variation of the instantaneous projected speeds which have two opposite phases: positive correlations at one side of the azimuthal angles and negative correlations at the other side.

where $\gamma$ is a drag parameter, $v$ is the CME speed, and $w$ is the ambient solar wind speed. The parameter $\gamma$ ($cm^{-1}$) is given by

$$\gamma = C_d \frac{A\rho_w}{m}, \quad (2)$$

where $C_d$ represents the dimensionless drag coefficient, $A$ is the cross-section area of the CME perpendicular to the direction of the propagation, $\rho_w$ is the ambient solar wind density, and $m$ is the CME mass. To estimate these parameters, we use Equations (3)–(6) of Vršnak et al. (2010). The mass of the CME was estimated

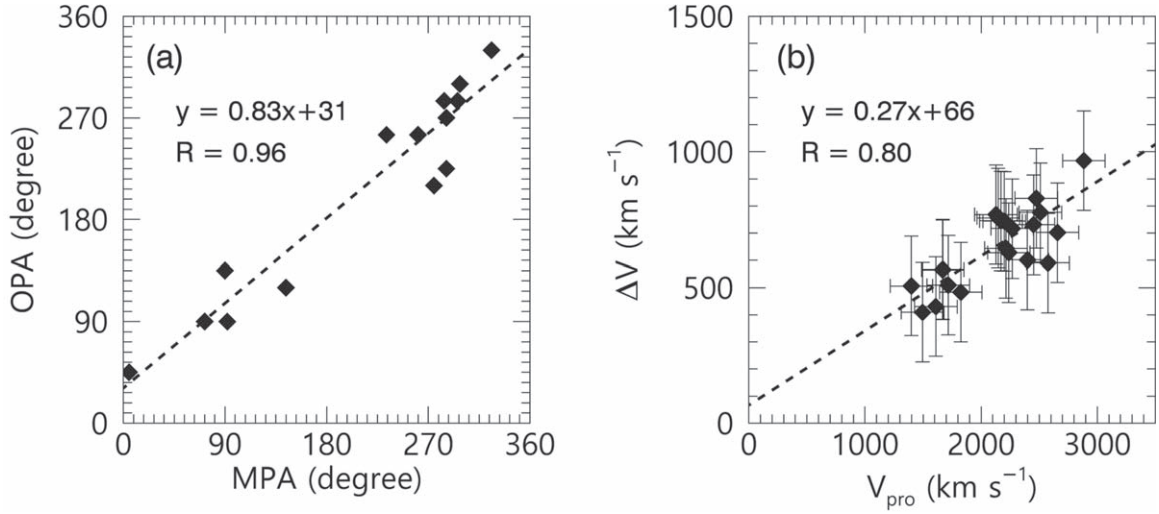


**Figure 6.** Correlations of various parameters of oscillating FHCMEs from LASCO C3: (a) MPA and OPA and (b) the observed maximum projected speed ($V_{pro}$) and the oscillation amplitude ($\Delta V$). The dashed lines indicate linear fits to the data. The error bars correspond to the standard deviations of the speeds from five independent measurements of the instantaneous height.

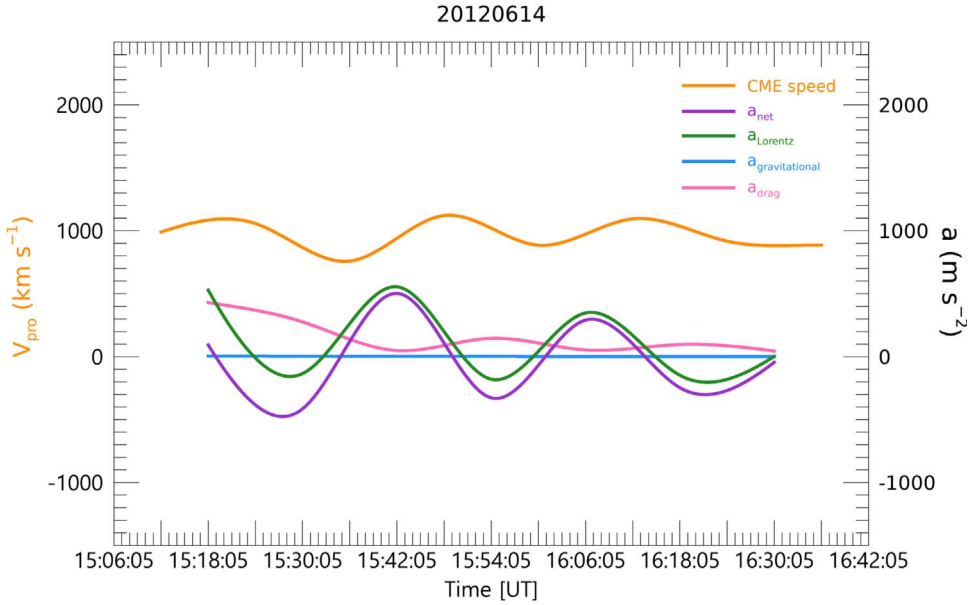


**Figure 7.** Profiles of the instantaneous projected speed and acceleration of the 2012 March 10 event from LASCO C3. The orange line indicates the maximum projected speed of the CME. The purple, green, blue, and pink curves correspond to the net, Lorentz, gravitational, and solar wind drag acceleration of the CME.

from brightness in the LASCO C3 images (for details see Vourlidas et al. 2000, 2010). The Lorentz acceleration can be estimated using $a_n$ estimated from the CME speed profile, the drag parameter $\gamma$ given by Vršnak et al. (2010), and $w = 400\,\mathrm{km\ s^{-1}}$. Figure 7 shows the instantaneous projected speed and the estimations of these three accelerations as a function of time for the analyzed event. As seen in the figure, Lorentz acceleration is dominant over the others so it can be approximated as the net acceleration, which is the derivative of CME speed. It is also noted that the effect of the drag force may be underestimated or overestimated due to the uncertainties of the drag coefficient and CME mass (Vourlidas et al. 2000, 2010; Sachdeva et al. 2015). Usually, the propagation phase of fast CMEs starts from a few solar radii (Vršnak 2006; Bein et al. 2011; Carley et al. 2012; Sachdeva et al. 2017). At large heights, the dynamics of CMEs has been assumed to be dominated by aerodynamic drag (Gopalswamy et al. 2000, 2001a; Vršnak & Gopalswamy 2002; Yashiro et al. 2004; Manoharan 2006; Tappin 2006; Vršnak & Žic 2007; Vršnak et al. 2008, 2010; Subramanian et al. 2012; Sachdeva et al. 2015; Takahashi & Shibata 2017). Our results are inconsistent with the assumptions of these past studies. We may conjecture that there is a global layer of enhanced current around the CMEs. Another possibility is that the kinematic oscillation is the result of the local or nonlinear nature of its driver as proposed by Nakariakov et al. (2009) and Takahashi et al. (2017).

## 4. Summary and Conclusion

Our study has shown the periodic variation of the instantaneous projected speed of FHCMEs, and allowed for determining the modes of the oscillation polarization, based on imaging coronagraph observations from different LoSs, obtained simultaneously with different spacecraft. We consider

21 FHCMEs, which were simultaneously observed by *SOHO* and *STEREO-A* and *-B* from 2010 June to 2012 August when the spacecraft were roughly in quadrature. We estimate the instantaneous speeds of the FHCMEs at 24 different azimuthal angles from the solar center in the plane of the sky. We find that all these FHCMEs have experienced quasi-periodic variations of the instantaneous projected velocity. The oscillation amplitude is found to correlate well with the projected speed. Durations of the observed oscillations are found to range from 48 to 120 min. The oscillation period ranges from 24 to 48 min with an average of 33.3 min. The range of the detected periods is restricted by the time resolution of the coronagraphs used, and the duration of the detection. The oscillations of 21 events are found to be associated with distinct azimuthal wave modes, and the $m = 1$ mode is dominant (13 events, 62%).

Properties of the kinematic oscillation patterns determined in this study, i.e., the periods, amplitudes, and durations, are similar to those reported by Krall et al. (2001), Shanmugaraju et al. (2010), Lee et al. (2015), and Michalek et al. (2016). In particular, Lee et al. (2015) determined projected azimuthal wave modes of nine HCMEs. However, previous studies of this phenomenon were performed from a single LoS only, with the LASCO coronagraph, which did not allow the authors to account for the projection effects in the identification of the azimuthal mode of oscillation. The present study, based on the use of observations of the oscillations from different LoSs with different spacecraft, reduces the ambiguity of the azimuthal wave number identification. The oscillations are found to be polarized in the direction of CME propagation. Oscillations of this polarization have already been detected at much smaller scale as vertical oscillations of a magnetic flux rope rising up in the corona (Kim et al. 2014). Estimations of the accelerations of the detected CMEs demonstrate that the effect of the Lorentz force is dominant over other forces such as gravity and the drag force. Thus, the magnetic force is likely to be responsible for the kinematic oscillations, and the oscillations could be modeled by the approach introduced in Cargill et al. (1994). On the other hand, the dependence of the oscillation amplitude on CME speed, confirmed by this study, indicates a nonlinear nature of the oscillations (Nakariakov et al. 2009; Takahashi et al. 2017), associated with the vortex-shedding phenomenon (Lee et al. 2015). However, the radial (vertical) polarization of the detected oscillations does not seem to be consistent with the intrinsically perpendicular (horizontal) direction of the vortex-shedding phenomenon (Nakariakov et al. 2009). Our findings indicate the need for further development of the theory of kinematic oscillations of CMEs, in particular accounting for their 3D nature and nonlinearity.

This work was supported by the BK21 plus program through the National Research Foundation (NRF) funded by the Ministry of Education of Korea, the Basic Science Research Program through the NRF funded by the Ministry of Education (NRF-2016R1A2B4013131), NRF of Korea Grant funded by the Korean Government (NRF-2013M1A3A3A02042232), the Korea Astronomy and Space Science Institute under the R&D program supervised by the Ministry of Science, ICT and Future Planning, the Korea Astronomy and Space Science Institute under the R&D program Development of a Solar Coronagraph on International Space Station (Project No. 2017-1-851-00) supervised by the Ministry of Science, ICT and Future Planning, and Institute for Information & communications Technology Promotion (IITP) grant funded by the Korea government(MSIP) (2018-0-01422, Study on analysis and prediction technique of solar flares). V.M.N. acknowledges STFC consolidated grant ST/P000320/1.

The *SOHO*/LASCO CME catalog (http://cdaw.gsfc.nasa.gov/CME_list/) is generated and maintained at the CDAW Data Center by NASA and the Catholic University of America in cooperation with the Naval Research Laboratory. *SOHO* is a project of international cooperation between ESA and NASA. The *STEREO*/SECCHI data are produced by an international consortium of the NRL, LMSAL and NASA GSFC (USA), RAL and University of Birmingham (UK), MPS (Germany), CSL (Belgium), IOTA and IAS (France).

## ORCID iDs

Harim Lee https://orcid.org/0000-0002-9300-8073
Y.-J. Moon https://orcid.org/0000-0001-6216-6944
V. M. Nakariakov https://orcid.org/0000-0001-6423-8286
Il-Hyun Cho https://orcid.org/0000-0001-7514-8171

## References

Bein, B. M., Berkebile-Stoiser, S., Veronig, A. M., et al. 2011, ApJ, 738, 191
Bronarska, K., & Michalek, G. 2018, AdSpR, 62, 408
Brueckner, G. E., Howard, R. A., Koomen, M. J., et al. 1995, SoPh, 162, 357
Cargill, P. J. 2004, SoPh, 211, 135
Cargill, P. J., Chen, J., & Garren, D. A. 1994, ApJ, 423, 854
Cargill, P. J., Chen, J., Spicer, D. S., & Zalesak, S. T. 1996, JGR, 101, 4855
Carley, E. P., McAteer, R. T. J., & Gallagher, P. T. 2012, ApJ, 752, 36
De Moortel, I., & Nakariakov, V. M. 2012, RSPTA, 370, 3193
Gopalswamy, N., Lara, A., Lepping, R. P., et al. 2000, GeoRL, 27, 145
Gopalswamy, N., Lara, A., Yashiro, S., Kaiser, M. L., & Howard, R. A. 2001a, JGR, 106, 29207
Gopalswamy, N., Yashiro, S., Kaiser, M. L., Howard, R. A., & Bougeret, J.-L. 2001b, JGR, 106, 29219
Gosling, J. T. 1993, JGR, 98, 18937
Gosling, J. T., McComas, D. J., Phillips, J. L., & Bame, S. J. 1991, JGR, 96, 7831
Kaiser, M. L., Kucera, T. A., Davila, J. M., St., et al. 2008, SSRv, 136, 5
Kim, S., Nakariakov, V. M., & Cho, K.-S. 2014, ApJL, 797, L22
Krall, J., Chen, J., Duffin, R. T., Howard, R. A., & Thompson, B. J. 2001, ApJ, 562, 1045
Lee, H., Moon, Y.-J., & Nakariakov, V. M. 2015, ApJL, 803, L7
Lindsay, G. M., Luhmann, J. G., Russell, C. T., & Gosling, J. T. 1999, JGR, 104, 12515
Liu, W., & Ofman, L. 2014, SoPh, 289, 3233
Manoharan, P. K. 2006, SoPh, 235, 345
Michalek, G., Shanmugaraju, A., Gopalswamy, N., Yashiro, S., & Akiyama, S. 2016, SoPh, 291, 12
Nakariakov, V. M., Aschwanden, M. J., & Van Doorsselaere, T. 2009, A&A, 502, 661
Sachdeva, N., Subramanian, P., Colaninno, R., & Vourlidas, A. 2015, ApJ, 809, 158
Sachdeva, N., Subramanian, P., Vourlidas, A., & Bothmer, V. 2017, SoPh, 292, 118
Shanmugaraju, A., Moon, Y.-J., Cho, K.-S., et al. 2010, ApJ, 708, 450S
Subramanian, P., Lara, A., & Borgazzi, A. 2012, GeoRL, 39, 19107
Takahashi, T., Qiu, J., & Shibata, K. 2017, ApJ, 848, 2
Takahashi, T., & Shibata, K. 2017, ApJL, 837, L17
Tappin, S. J. 2006, SoPh, 233, 233
Vourlidas, A., Howard, R. A., Esfandiari, E., et al. 2010, ApJ, 722, 1522
Vourlidas, A., Subramanian, P., Dere, K. P., & Howard, R. A. 2000, ApJ, 534, 456
Vršnak, B. 2006, AdSpR, 38, 431
Vršnak, B., & Gopalswamy, N. 2002, JGRA, 107, 1019
Vršnak, B., Ružicdjak, D., Sudar, D., & Gopalswamy, N. 2004, A&A, 423, 717
Vršnak, B., Vrbanec, D., & Čalogović, J. 2008, A&A, 490, 811
Vršnak, B., & Žic, T. 2007, A&A, 472, 937
Vršnak, B., Žic, T., Falkenberg, T. V., et al. 2010, A&A, 512, 43
Yashiro, S., Gopalswamy, N., Michalek, G., et al. 2004, JGRA, 109, 7105